A00-16424

AIAA 2000-0547

Micromachined Acoustic Resonators for Microjet Propulsion

Michael O. Müller, Luis P. Bernal
Robert P. Moran, Peter D. Washabaugh
Department of Aerospace Engineering

Babak Amir Parviz, Khalil Najafi
Department of Electrical Engineering and
Computer Sciences

University of Michigan
Ann Arbor, MI 48109-2140

38th Aerospace Sciences Meeting & Exhibit
10-13 January 2000 / Reno, NV

AIAA-2000-0547

MICROMACHINED ACOUSTIC RESONATORS FOR MICROJET PROPULSION

Michael O. Müller[§], Luis P. Bernal[*], Robert P. Moran[§], Peter D. Washabaugh[*]
Department of Aerospace Engineering

Babak Amir Parviz[†], Khalil Najafi[‡]
Department of Electrical Engineering and Computer Science

University of Michigan
Ann Arbor, Michigan 48109-2140

ABSTRACT

The thrust produced by synthetic jets designed for micro jet propulsion is discussed. The proposed propulsion system consists of synthetic wall jets located at the throat of an ejector shroud that are powered by Helmholtz-type acoustic resonators. The theory of acoustic resonators is described and the thrust produced by the resonators calculated. Theoretical results of the exit velocity and thrust are in good agreement with experimental measurements obtained using particle image velocimetry (PIV) in an axisymmetric synthetic jet. Theoretical results are shown to predict well the resonant frequency of a 10:1 scale model of a micromachined resonator. The thrust produced by the micro scale devices is discussed. It is shown that the micro scale devices could be used as propulsion units for Micro Airborne Platforms (MAP).

INTRODUCTION

There is a great deal of interest on micro scale jets capable of producing large impulse for application to flow control and propulsion. Streaming produced by a large amplitude acoustic field can be used to produce a synthetic jet stream. A very attractive feature of synthetic jets is that the mean mass flow at the source is zero and therefore the jet stream is produced without the need for an air supply. Several investigations have documented the flow field associated with acoustic streaming.[1,2] Synthetic jets have also been implemented using Micro Electro-Mechanical Systems (MEMS) fabrication methods.[2, 3] Glezer and co-workers[4] have demonstrated the use of synthetic jets for flow control applications. Dauphinee[5] describes an acoustic air pump with performance comparable to mechanical fans. This particular application illustrates the large entrainment associated with acoustic streaming. However, the use of acoustic streaming for propulsion has not been investigated.

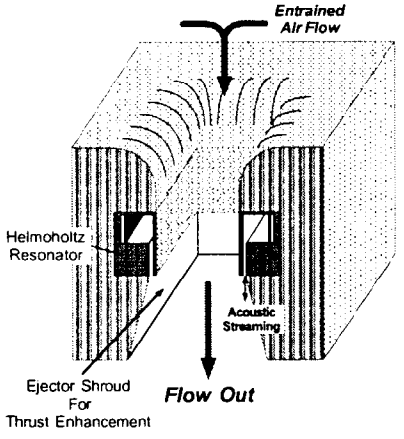

Figure 1. Conceptual drawing of a micromachined acoustic ejector (MACE). (a) Illustration a thruster unit. (b) Schematic diagram of a micromachined acoustic resonator.

§ Graduate Research Assistant, Department of Aerospace Engineering, Member AIAA.
* Associate Professor, Department of Aerospace Engineering, Senior Member AIAA.
† Graduate Research Assistant, Department of Electrical Engineering and Computer Science.
‡ Professor, Department of Electrical Engineering and Computer Science.

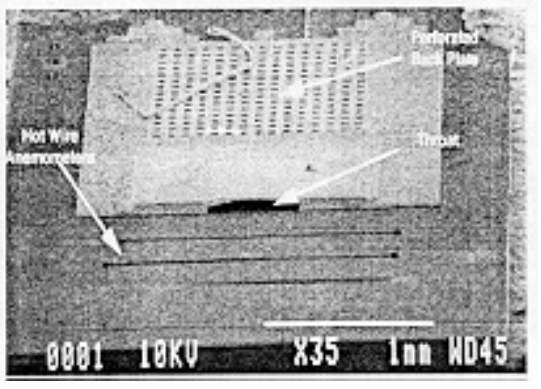

Figure 2. SEM picture of a micromachined acoustic resonator

The main focus of the present research is a new propulsion concept for micro airborne platforms. The concept is illustrated in figure 1. A thruster unit or MACE consists of acoustic resonators with the throat exit located in an ejector shroud. The resonator generates a large amplitude acoustic field that in turn produces a synthetic jet. The arrangement produces thrust equal to the momentum flux of the synthetic jet. In addition, entrainment and mixing in the ejector shroud augments the thrust of the system. Several resonators have been designed and fabricated using MEMS techniques at the University of Michigan Center for Integrated Micro Systems. The device shown in Figure 1 consists of a cavity and throat. The throat is oriented parallel to the wall producing a synthetic wall jet. An electro-statically driven diaphragm produces the acoustic field inside the resonator. The back electrode is perforated to minimize damping. A scanning electron micrograph (SEM) image of a micromachined resonator is shown in Figure 2. This device has a throat area 30 μm × 500 μm and the drive diaphragm area is 1.2 mm × 1.2 mm. Details of the design and the MEMS fabrication process can be found in reference [6].

In this paper we derive the theory of acoustic resonators with an emphasis on the thrust performance. Acoustic resonators have been the subject of numerous investigations since the early work by Helmholtz[7] and Rayleigh.[8] Of particular interest to the present research is the acoustic impedance of the resonator throat at large amplitudes and frequency. Ingård and Labate[1] report observations of the flow field associated with large amplitude velocity oscillations in an orifice. They identified several flow regimes and report "phase diagrams" to characterize the effect of various relevant parameters. At large flow velocities they observed the formation of a series of vortex rings that propagate away from the orifice.

At the amplitudes of interest here the acoustic impedance of the resonator throat is not constant. The nonlinear acoustic impedance of an orifice has been the subject of many investigations. Panton and Goldman[9] provide a compilation of the data available in the literature and give a detail discussion of the effect of velocity fluctuation amplitude on the resistance and reactance of circular orifices. The correlation results show that at large velocity the resistance of the orifice increases linearly with speed while it is approximately constant at low speed. The transition between these two regimes occurs at non-dimensional velocity $V/\sqrt{\nu\omega}$ of order one. The correlation values for the reactance are in good agreement with the theoretical results of Rayleigh[8] at low speed, and decrease at large velocity.

In what follows we first derive a theory of acoustic resonators and develop equations for the thrust produced by the resonator. We present also the results of experimental studies conducted to validate the theory and to determine the actual performance and relevant scaling laws of the devices.

ACOUSTIC RESONATOR THEORY

A reduced order model of the complex processes in an acoustic resonator intended for use as a propulsion unit in micro air platforms has been developed. The theoretical model is intended for use as a guide to identify the design parameters of the resonator and to determine target values for those parameters. Scaling laws could also be developed based on the model. Scaling laws are the basis for trade off diagrams to improve the performance of acoustic resonators designed for thrust generation.

The main assumption of the theory is that the wavelength of the acoustic field is large compared to the larger dimension of the resonator. This implies that the pressure in the resonator cavity is uniform. The resonator operates in the first acoustic mode. This assumption puts an upper bound on the maximum frequency that can be modeled accurately. At high frequencies higher order spatial modes could become dominant. These modes have a non-uniform pressure distribution in the cavity. In order to accurately predict the resonator performance the spatial structure of the relevant mode is needed. The spatial structure of the acoustic field associated with higher order modes adds a complicating factor to the design of the resonator since in this case the location of the diaphragm and output throat must be suitable positioned relative to the spatial structure of the mode in order to minimize losses. For the first acoustic mode assumed here the

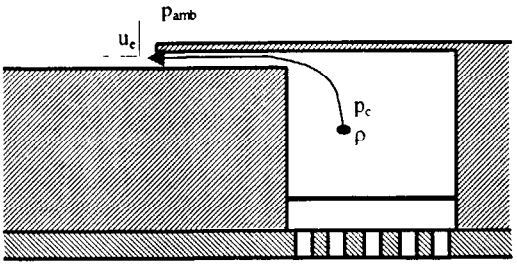

Figure 3. Streamline during outflow part of cycle.

performance of the resonator is not influenced by the location of the diaphragm or output throat.

The main flow feature of the resonator is the unsteady motion of air in and out of the cavity. From the point of view of the fluid mechanics of thrust generation, the key assumption is that boundary layer separation at the throat exit causes a topological change of the streamlines. This flow separation phenomenon is clearly observed in the smoke visualization of Ingård and Labate[1] at high flow velocity. These observations cannot be explained by classical acoustic streaming theory that assumes small amplitude oscillatory motion without topological changes of the flow field. Correlations of the type developed by Panton and Goldman[10] incorporate the most important aspects of the nonlinear effects associated with high exit velocities. However, the thrust produced by the resonator can only be determined after the topological change of the streamlines is taken into.

The theoretical model presented here is developed from fundamental principles. The results are then interpreted based on empirical correlation available in the literature. The resonator model is cast in terms of inertia, compliance, damping and forcing terms. Inertia terms are associated with the air mass in oscillatory motion in and around the throat. Damping terms are caused by friction in the throat and orifices, and by boundary layer separation effects. The compliance terms are associated with compressibility of the air mass in the resonator cavity. The forcing term results from the volume displaced by the diaphragm.

Resonator Apparent Mass and Damping

The flow through the resonator throat determines the apparent mass and damping of the resonator. The air mass engaged in oscillatory motion in the throat and cavity determines the apparent mass of the resonator. Friction losses in the throat and flow separation at the exit plane of the throat cause damping. The line integral of the momentum equation along a streamline

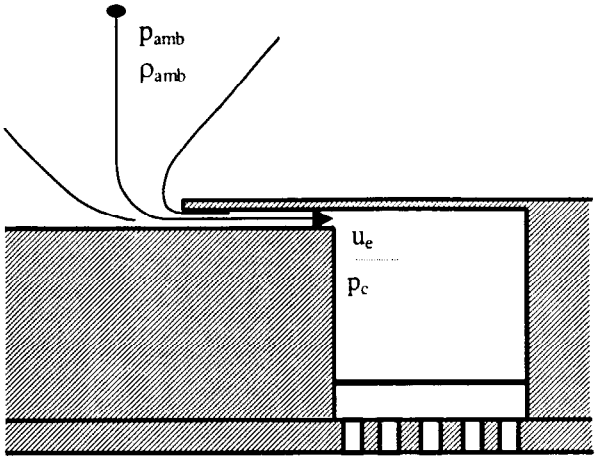

Figure 4. Flow streamlines during inflow to the cavity.

relates the throat exit velocity to the pressure in the cavity.

For the outflow part of the cycle, a typical streamline originates in the resonator cavity as shown in Figure 3. Boundary layer separation occurs at the exit plane of the throat. Depending on the detail design of the throat, particularly for short throats, the streamlines as the flow leaves the throat might curve. The line integral is evaluated between the cavity and the exit plane of the throat as shown in Figure 2. The flow is assumed incompressible, i.e. u small compared to the speed of sound. Thus,

$$\rho \frac{d}{dt} \int \vec{u}\cdot d\vec{s} + \rho \int \nabla\left[\frac{\vec{u}^2}{2} + p\right]\cdot d\vec{s} \quad \text{..... (1)}$$
$$= -\mu \int (\nabla \wedge \vec{\omega})\cdot d\vec{s}$$

The resulting equation after integration is

$$\frac{du_e}{dt} = \frac{1}{L_E}\frac{p}{\rho} - \frac{u_e^2}{2C_D^2 L_E} - 8\frac{\mu}{\rho}\frac{u_e}{h_T^2}\frac{L_v}{L_E},\ u_e \geq 0 \quad \text{..... (2)}$$

where:

$u_e(t)$ is the maximum velocity at the exit plane of the resonator,

$p(t) = p_c - p_{amb}$ is the relative pressure in the resonator cavity,

$\rho(t)$ is the air density in the resonator cavity,

μ is the air viscosity,

h_T is the resonator throat height,

L_E is the equivalent inertia length of the throat,

L_v is the equivalent viscous length of the throat,

C_D is a flow coefficient associated with the streamline curvature at the exit plane of the throat.

For the inflow part of the cycle, typical streamlines are shown in Figure 4. Boundary layer separation causes the pressure to be uniform at the throat-cavity interface and equal to the cavity pressure. In this case the line integral is evaluated between ambient conditions and the exit plane of the throat in the cavity giving,

$$\frac{du_e}{dt} = \frac{1}{L_E}\frac{p}{\rho_{amb}} + \frac{u_e^2}{2C_D^2 L_E} - 8\frac{\mu}{\rho_{amb}}\frac{u_e}{h_T^2}\frac{L_v}{L_E}, \quad u_e < 0 \quad .....(3)$$

where ρ_{amb} is the ambient density. We assume also that the equivalent lengths L_E and L_v for the inflow and outflow part of the cycle are equal. This is justified by the observation that these equivalent lengths scale with the geometrical length, L_T, and cross section area, A_T, of the throat.

Rayleigh[8] suggested that the contribution to L_E of the air mass in the throat and outside the throat is additive. Hence the equivalent length of the throat can be written as,

$$L_E = L_T + \frac{(\pi A_T)^{1/2}}{4} \quad .....(4)$$

where A_T is the cross section area of the throat. The second term in this equation accounts for the inertia of the air mass in oscillatory motion outside the throat. Helmholtz[7] first evaluated this term for a circular orifice. Here we assume flow separation at the exit of the throat and therefore the contribution is half the value derived by Helmholtz. Rayleigh[8] showed that the equivalent length for one side of a circular orifice is between $\pi D/8$ and $8D/(3\pi)$, where D is the orifice diameter.

The effect of the throat cross-section shape on the equivalent length is more difficult to characterize. It only affects the second term in equation (4). Rayleigh[8] discusses the effect of aspect ratio for elliptical cross section orifices. More recently, Chanaud[10] discusses the effect of orifice geometry on the resonance frequency of acoustic resonators. Here we use the orifice equation with diameter equal to the diameter of an orifice of the same cross sectional area as the throat. This is the value given in equation (4).

Damping is associated with the last two terms on the right hand side of equations (2) and (3). The first damping term is proportional to the square of the exit velocity and results from flow separation at the throat exit. The flow coefficient C_D is introduced to account for the curvature of streamlines near separation. Friction in the throat is characterized by L_v, the equivalent viscous length of the throat. The magnitude of L_v a function of the flow Reynolds number, $\mathrm{Re} = \frac{\rho\omega h_T^2}{\mu}$. At high Reynolds number (i.e. at high frequency), $\mathrm{Re} >> 1$, the flow along the axis of the throat is irrotational and $L_v \approx 0$. In general, L_v is always smaller than the throat length L_T. It depends on the ratio h_T/L_T and the flow Reynolds number. For $h_T/L_T << 1$ and $\mathrm{Re} \approx 1$, $L_v/L_T \approx 1$. The numerical coefficient in the viscous friction term in equations (2) and (3) is valid only for a two-dimensional throat geometry (i.e. $A_T >> (h_T)^2$).

Resonator Compliance and Forcing

The resonator compliance and the forcing term are obtained by considering conservation of mass in the cavity.

$$\frac{d}{dt}(\rho V) = -\rho u_e A_E \quad .....(5)$$

where A_E is the effective area of the throat and V is the cavity volume. We note that the air density equals the ambient density during the inflow part of the cycle, while the density equals the resonator cavity density during the outflow part of the cycle. It follows assuming isentropic compression of the air mass in the cavity,

$$\frac{dp}{dt} = a^2\frac{d\rho}{dt} = -\rho a^2\frac{u_e A_E}{V} - \rho a^2\frac{1}{V}\frac{dV}{dt}, \quad u_e \geq 0 \quad .....(6)$$

$$\frac{dp}{dt} = a^2\frac{d\rho}{dt} = -\rho_{amb} a^2\frac{u_e A_E}{V} - \rho a^2\frac{1}{V}\frac{dV}{dt}, \quad u_e < 0 \quad .....(7)$$

where a is the speed of sound. The first term on the right hand side determines the cavity compliance. The second term models the forcing due to the diaphragm motion.

The effective area of the throat, A_E, is always less than the geometrical area, A_T, because of viscous effects. At high Reynolds number $A_E \approx A_T$. There is only a small correction due to the thin viscous region at the wall. At low Reynolds number viscous effects dominate. A parabolic velocity profile develops in the throat which gives $A_E = 2/3\ A_T$ for a two-dimensional throat geometry.

The displacement of the diaphragm causes a volume change that drives the resonator cavity flow. The volume displaced by the diaphragm is given by

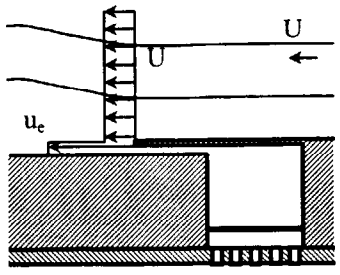

(a)

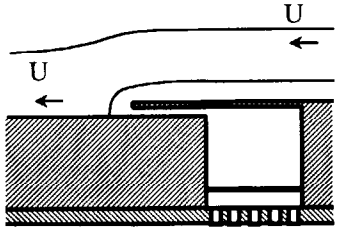

(b)

Figure 5. Schematic diagram of the streamlines outside the resonator for a free stream velocity U. (a) Flow topology during outflow. (b) Flow topology during inflow.

$$V_D(t) = \int_0^{L_D}\int_0^{L_D} \eta(x,y,t)\ dx\ dy \quad \text{.....(8)}$$

The diaphragm shape during oscillation is assumed to be of the form,

$$\eta(x,y,t) = h_D(t)\sin\left(\frac{\pi x}{L_D}\right)\sin\left(\frac{\pi y}{L_D}\right) \quad \text{.....(9)}$$

where a square diaphragm has been assumed with h_D the displacement at the center of the diaphragm and L_D the size of the diaphragm. Then,

$$V_D(t) = \frac{4}{\pi^2} A_D h_D(t) \quad \text{.....(10)}$$

The resonator cavity volume is then

$$V(t) = V_C - V_D(t) = V_C - \frac{4}{\pi^2} A_D h_D(t) \quad \text{.....(11)}$$

where V_C is the resonator cavity volume with the diaphragm at the equilibrium position. The rate of change of the volume is

$$\frac{dV}{dt} = -\frac{dV_D}{dt} = -\frac{4A_D}{\pi^2}\frac{dh_D}{dt} \quad \text{.....(12)}$$

Thrust

The thrust produced by the resonator can be evaluated by considering conservation of momentum for the flow outside the resonator. Figure 5a shows the flow topology for the outflow part of the cycle. The time integral of the momentum flux divided by the period of oscillation gives a positive contribution to the mean thrust

$$J = \frac{1}{T}\int_{u_e>0}\int_{A_T} \rho\ u^2\ dA\ dt = \frac{1}{T}\int_{u_e>0} \rho\ u_e^2\ A_{JE}\ dt \quad \text{....(13)}$$

where T is the period of the oscillation, and A_{JE} is the effective area of the throat for thrust. At high Reynolds number the effective area of the throat equals the geometrical area except for boundary layer effects which are generally small, i.e. $A_{JE} = A_T$. At low Reynolds number the effective area for a two-dimensional throat geometry is $A_{JE} = 8/15\ A_T$.

Figure 4b shows the flow topology during the inflow part of the cycle. Momentum balance shows that there is drag associated with the inflow into the resonator. A control volume analysis gives

$$D = -\frac{1}{T}\int_{u_e<0}\int_{A_T} \rho_{amb}\, U\, dA\, dt = -\frac{\rho_{amb} U}{T}\int_{u_e<0} u_e A_E dt \quad \text{....(14)}$$

where U is the flow speed outside the resonator, and A_E is the effective area for mass flow introduced in above. Note that for U = 0 the drag associated with the inflow is zero. The mean thrust acting on the resonator is, therefore,

$$T_h = J - D = \frac{1}{T}\left(\int_{u_e>0} \rho u_e^2 A_{JE} dt + \rho_{amb} U \int_{u_e<0} u_e A_E dt\right) \quad \text{.(15)}$$

Acoustic Streaming

Several criteria could be used to characterize the efficiency of the resonator from the point of view of acoustic streaming and thrust generation. The fact that at large speeds the flow is characterized by a sequence of vortex ring suggests that the total vorticity introduced into the flow field during the outflow part of the cycle is an important parameter. The flux of vorticity at the exit cross-section of the throat is given by

$$\int_{wall}^{centerline} u\ \frac{\partial u}{\partial n}\ dn = \frac{u_e^2}{2} \quad \text{.....(16)}$$

Hence, the total amount of vorticity (i.e. circulation) produced by the resonator in a cycle is

$$\Gamma = \int_{u_e>0} \frac{u_e^2}{2}\, dt \quad \text{.....(17)}$$

A criterion for efficient thrust generation would be that the Reynolds number based on the circulation is large, i.e.

$$Re_S = \frac{\rho_{amb}\,\Gamma}{\mu} >> 1 \quad \text{.....(18)}$$

The actual magnitude of the Reynolds number would have to be determined based on experiments. Unsteady vortex ring flows suggest typical values for the Reynolds number $Re_S \approx 100$ or larger.

A second important consideration is the volume of fluid undergoing oscillatory motion in the throat of the resonator. This volume should be equal to or larger than the equivalent throat volume in order for vortex ring formation to occur. The amount of mass in oscillatory motion is

$$M = -\int_{u_e<0}\int_{A_j} \rho_{amb}\, u\, dA\, dt = -\rho_{amb}\int_{u_e<0} u_e A_E\, dt \quad \text{.....(19)}$$

Therefore introducing the flow length L_f defined as

$$L_f = \int_{u_e<0} u_e\, dt \quad \text{.....(20)}$$

a condition for efficient streaming and thrust generation might be expressed as

$$\frac{M}{\rho_{amb} A_E L_E} = \frac{L_f}{L_E} = -\frac{1}{L_E}\int_{u_e<0} u_e\, dt \geq 1 \quad \text{.....(21)}$$

A more precise criterion could be developed based on recent experiments on the formation of vortex ring by Gharib and coworkers.[11] These experiments show that there is an optimum flow length for the formation of vortex rings. The optimum value is approximately 5 diameters. These vortex ring results would suggest that optimum performance might be obtained for L_f/h_T a constant of order one, possibly equal to 5 for an axisymmetric configuration.

Numerical Solution

In order to obtain the behavior of the resonator, equations (2), (3), (6) and (7) are solved using an off-the-shelf ODE solver (MATLAB). Equations (2) and (6) are used when u_e is positve (outflow) and equations (3) and (7) are used when u_e is negative (inflow). Input parameters are the geometry of the resonator and the amplitude of the diaphragm motion. All the results reported here were obtained for a sinusoidal temporal variation of the diaphragm displacement. Input parameters are:

V_C cavity volume,

A_D diaphragm area,

h_o diaphragm displacement at the center,

f frequency,

A_T throat cross section area,

$A_E = A_T$,

h_T throat height,

L_T throat length,

L_v equivalent viscous length of the throat,

μ air viscosity,

a. speed of sound.

The system of equations describing the resonator is a second order system with a non-linear damping term. The resonance frequency is given by,

$$f_o = \frac{a}{2\pi}\sqrt{\frac{A_E}{L_E V_c}} \quad \text{.....(22)}$$

This result was first derived by Helmholtz.[7] In a typical calculation u_e, p, are ρ are evaluated as a function of time until the initial transient subsides. When the steady state is reached, the results are used to calculate the thrust T_h and the flow length L_f.

EXPERIMENTAL RESULTS

Several experiments are being conducted to validate the theoretical results. Below we describe results obtained using an axisymmetric synthetic jet and a 10:1 scale model of the micromachined resonator shown in figure 2.

Axisymmetric Synthetic Jet Results

The objective of these experiments is to determine the performance of the resonator and synthetic jet using PIV measurements of the flow field at various phases of the acoustic cycle and for several frequencies. The PIV velocity field measurements are used to determine the momentum flux in the synthetic jet plume and thus provide a measurement of the thrust. In this paper we briefly outline the methods and results. A more detailed account of these results will be provided elsewhere[12]. Figure 6 is a schematic diagram of the axisymmetric synthetic jet. It uses a loudspeaker diaphragm to drive the flow. The synthetic jet system is a 203 mm diameter loudspeaker cone attached to a

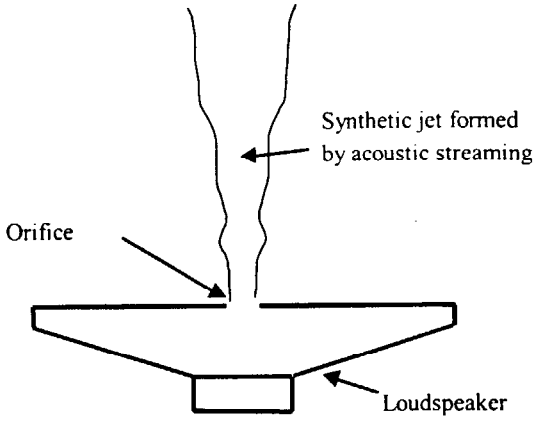

Figure 6. Schematic diagram of large scale resonator experiment.

thin cavity and a plate containing the orifice. The orifice is a sharp edged 12.7 mm diameter hole in a 3.2 mm thick plate. The loudspeaker cone position is measured with an optical position probe. The jet is shielded from ambient room currents on three sides and above with black foamcore, and with a clear plastic viewing window in front. The geometrical parameters of the synthetic jet apparatus relevant to the theoretical model are listed below:

V_C = 1400 cm^3,

A_T = 127 mm^2,

h_T = 12.7 mm,

L_T = 3.2 mm,

The resonance frequency is f_o = 180 Hz. The volume displaced by the diaphragm at the frequencies tested is given in Table 1. In these experiments the voltage amplitude into the loudspeaker was kept constant.

Table 1

f (Hz)	10	20	40	60	80	100
V_D(cm^3)	30	20	11	6.8	5.2	4.8

Two image PIV is used to measure the velocity field. The flow is seeded with smoke from the nebulizer, and illuminated with a laser sheet formed from the output of two Nd-YAD lasers operated at 532 nm wavelength. Images are taken with a high-resolution digital camera. The time between pictures is varied, such that smoke particles moved by O(1) pixels between images. Data is taken at 10, 20, 40, 60, 80, and 100 Hz. Beyond 100 Hz, the displacement of the loudspeaker is significantly reduced, and the jet is barely, physically, felt. At each frequency five

Figure 7. PIV image of resonator output flow showing the formation of a vortex ring. The fluid ejected from the orifice is visualized because it has a lager concentration of seed particles. The loudspeaker was operated at 20 Hz, and the speaker volume displacement was 20 cm^3. Phase: 90°.

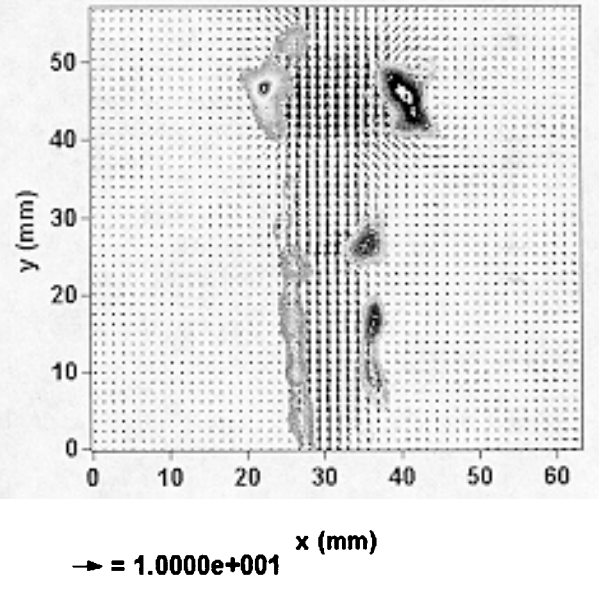

Figure 8. Velocity field during the output part of the diaphragm cycle. Contour lines superposed on the vector plot give the vorticity distribution. Flow conditions are the same as in Figure 7.

realizations of the flow are recorded at 0, 45°, 90°, 135°, 180°, 235°, 270°, 315° and 360° phase.

The PIV data is analyzed by a cross correlation algorithm, resulting in a velocity field from the nozzle

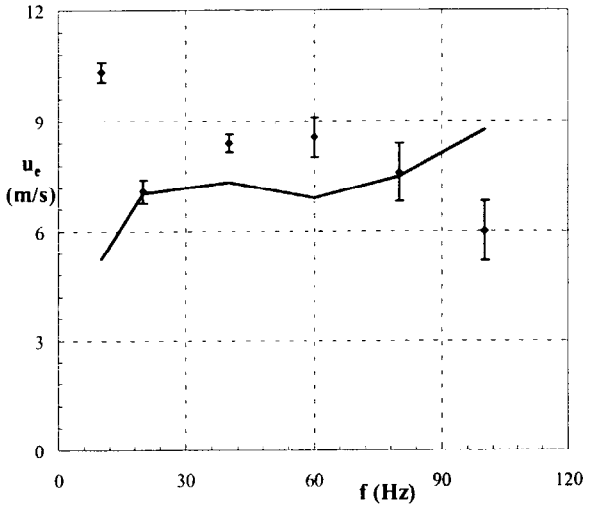

Figure 9. Plot of the measured output velocity at different frequencies (symbols). For these experiments the input voltage to the loudapeaker was kept constant. The solid line is the computed output velocity for the measured loudspeaker cone displacement

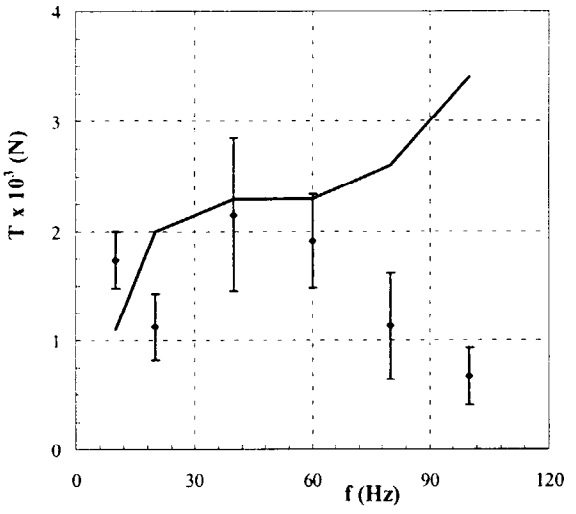

Figure 10. Model predictions for jet impulse as function of operating frequency. Solid line – model predictions. Diamonds – experimental results.

to five nozzle diameters downstream, and six diameters wide (centered about the nozzle). From the velocity data, vorticity, momentum flux, and impulse are calculated through a complete cycle of the loudspeaker diaphragm. A typical flow picture obtained at 20 Hz and 90° phase is shown in Figure 7. The fluid in the resonator cavity has a larger concentration of particles than the surrounding fluid. A vortical structure formed by acoustic streaming is found some distance away from the orifice. Figure 8 shows the velocity vector plot and vorticity contours at the same conditions as Figure 7. The vorticity contours confirm that the structure observed in the flow visualization is indeed vortical. In addition there is some vorticity along the vertical column of fluid ejected from the resonator.

Figures 9 and 10 show comparisons of the predicted exit velocity and thrust of the resonator with the measured values. For these test the loudspeaker was operated at constant voltage and therefore the amplitude of the diaphragm motion varied with frequency. The calculated mean velocity and thrust we obtained using the measured amplitude of the loudspeaker motion. Given the simplicity of the theoretical model and the fact that the measurement uncertainty is significant, there is generally good agreement between the theory and experiments. The trend of data at high frequency is disturbing since the experiment show a reduction of velocity and thrust with frequency, while theory predicts an increase.

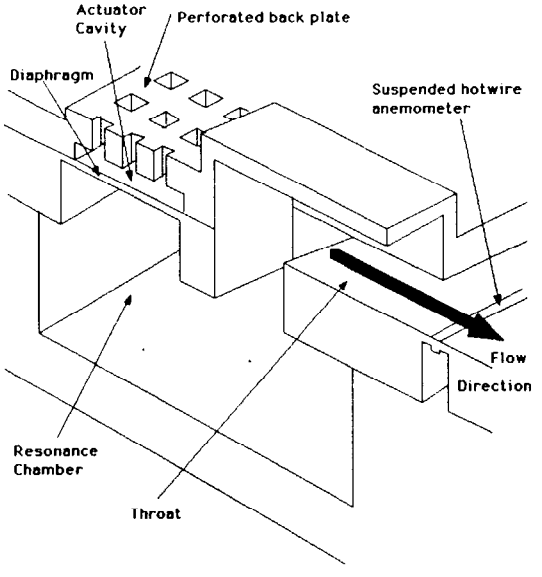

Figure 11. View of micromachined synthetic jet geometry. [6]

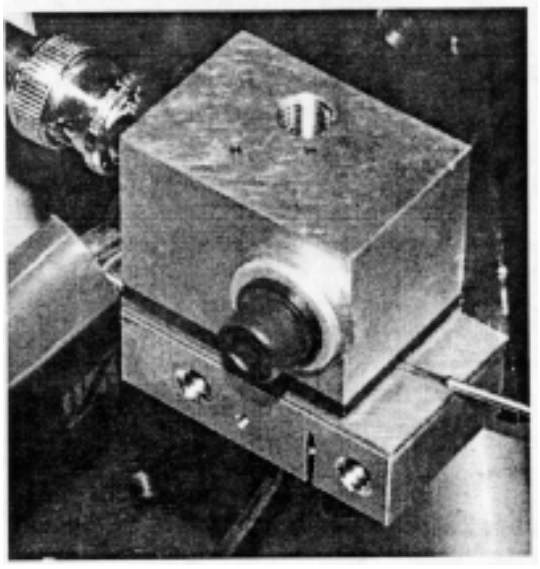

Figure 12. 10:1 scale model, showing hot wire anemometer probe at the throat.

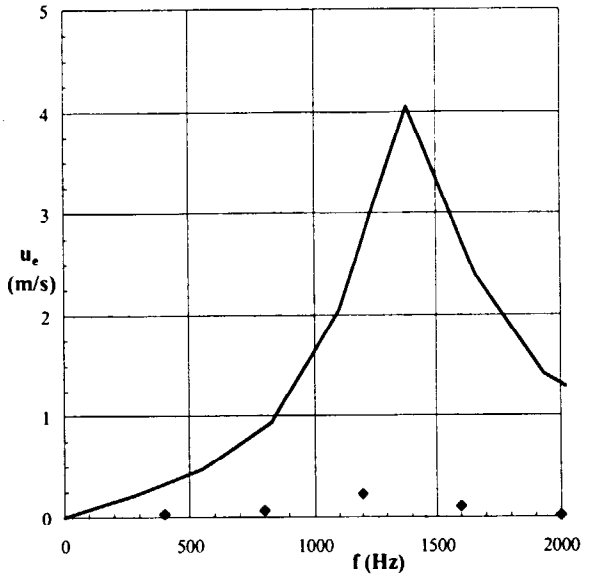

Figure 13 Model predictions for peak nozzle exit velocity as function of operating frequency. Solid line – model predictions, left axis. Diamonds – experimental results, right axis.

10:1 Scale Model Tests

The micromachined device is the primary focus of the current research. This configuration is more complex, in that the nozzle is no longer a straight channel. The details of the design are shown in Figure 11. The 10:1 scale model of the micromachined prototype manufactured using conventional fabrication methods is shown in Figure 12. The photograph shows a hot wire anemometer probe used to measure the exit flow velocity. The flow is produced by an electro statically driven membrane. The position of the membrane at the center is measured using a fiber optical probe simultaneously with the throat exit velocity.

The geometrical parameters of the 10:1 scale model relevant to the theoretical model are listed below:

$V_C = 0.75\ cm^3$,

$A_T = 1.5\ mm^2$,

$h_T = 0.3\ mm$,

$L_T = 1.5\ mm$,

$V_D = 0.0233\ mm^3$.

The resonance frequency is f_o = 1,380 Hz. Note the very small value of the volume displaced by the membrane.

Figure 13 shows the predicted and measured velocity for the 10:1 scale of the micromachined device. For these predictions, the effective flow length is assumed to be equal to the potential flow assumption. Also, the nozzle flow is assumed to be fully viscous. In this case the experiments were conducted at the same peak to peak amplitude of membrane displacement for all frequencies. The measured resonance frequency, and the general shape of the graph are consistent with predictions. However, the measured velocities deviate from the predicted values by an order of magnitude. The shape of the membrane under load is not known. The present experimental configuration only allows measurement of the membrane position at the center of the membrane. There is evidence suggesting that the assumed sinusoidal deformation of the membrane during oscillation may not occur.

These results confirm the theoretical prediction of the resonance frequency. Further tests are needed to fully characterize the deformation of the membrane under dynamic load conditions. Uncertainty on the actual volume displaced by the membrane is believed to account for the lack of agreement of the velocity magnitude.

MICROMACHINED RESONATORS PERFORMANCE

The theoretical model was used to predict the performance of micromachined resonators. Two designs have been completed. The prototype design is

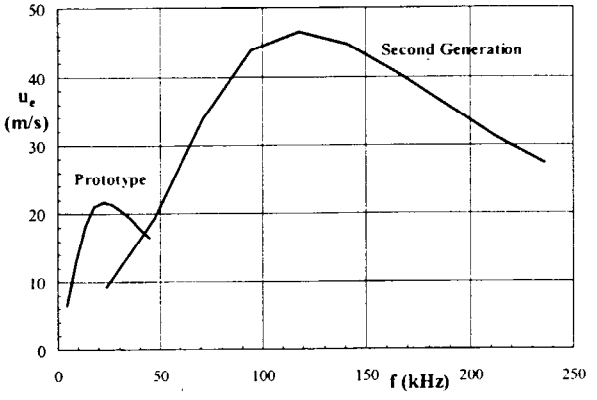

Figure 14. Predicted throat exit velocity for the micromachined resonators.

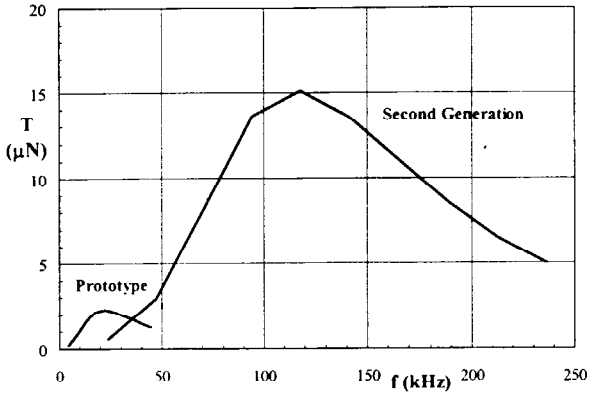

Figure 15. Predicted thrust for the micromachined resonators

shown in figure 2. The second generation device is a wafer integrated design with over 900 resonators. Each resonator has two throats.[13] The geometry of these designs is given in Table 2.

Table 2

	V_c (mm^3)	A_T (mm^2)	h_T (mm)	L_T (mm)	V_D (mm^2)	f_o (kHz)
Prototype	0.288	0.015	0.03	0.15	0.0018	22
2nd Gen	0.076	0.022	0.015	0.015	0.0018	180

The resonator exit velocity as a function of drive frequency is given in Figure 14. The resonator thrust is given in Figure 15. The second generation device is designed to produce significantly larger thrust, of the order of 27 mN for the entire device. Depending the amount of thrust augmentation by the ejector shroud. the device could produce sufficient thrust to lift the wafer. It should be noted that the second generation device is designed to operate at conditions well beyond the regimes tested in large scale tests.

CONCLUDING REMARKS

A theoretical model of acoustic resonators was described. The model is accurate for simple geometries. For more complex geometries, the model predicts well the resonance frequency but under predicts by an order of magnitude the peak velocity fluctuation. Recent evidence suggests that the effective membrane deflection in these tests could be significantly less than the values used in the calculations.

The model was used to determine the performance of micromachined resonators. These devices operate at very large frequency and can produce very large exit velocities. These calculations suggest that synthetic jets can be used for propulsion of micro airborne platforms.

REFERENCES

[1] INGÅRD, U. AND LABATE, S. 1950 Acoustic Circulation Effects and the Nonlinear Impedance of Orifices. *The Journal of the Acoustical Society of America.* **22**, 211-218

[2] COE, D.J., ALLEN, M.G., TRAUTMAN, M., AND GLEZER, A. 1994 Micromachined Jets for Manipulation of Macro Flows. *Proceedings of Solid State and Sensor Workshop.*

[3] COE, D.J., ALLEN, M.G., SMITH, B.L., AND GLEZER, A. 1995 Addressable Micromachined Jet Arrays. *Proceedings of Transducers.*

[4] SMITH, B. L. AND GLEZER, A. 1997 Vectoring and small-scale motions effected in free shear flows using synthetic jet actuators. *AIAA paper 97-0213.*

[5] DAUPHINE, T. M. 1957 Acoustic Air Pump. *Rev .Sci. Inst.***28**, 452.

[6] PARVIZ, B.A., BERNAL, L.P., AND NAJAFI, K. 1999 A Micromachined Helmholtz Resonator for Generation of Microjet Flows. *Proceedings of Transducers.*

[7] HELMHOLTZ, H. 1860 Theorie der luftschwingungen in rohren mit offenen enden.. *Crelle*

[8] RAYLEIGH, J. W.S.. 1945 The theory of sound Vol. II. Sec. 303-309. Dover.

[9] PANTON, R.L. AND GOLDMAN, A. L. 1976 Correlation of nonlinear orifce impedance. *J. Acoust. Soc. Am.* **60**, 1390-6

[10] CHANAUD, R. C. 1994 Effects of geometry on the resonance frequency of Helmholtz resonators. *J. Sound and Vibration.***178**, 337-48.

[11] GHARIB, M., RAMBOD, E. AND SHARIFF, K. 1998 A universal time scale for vortex ring formation. *J.Fluis Mech.* **360**, 121.

[12] MÜLLER, M.O., BALKANYI, S. AND BERNAL, L. P. 2000 Thrust performance of axisymmetric synthetic jets. In preparation

[13] B. A. PARVIZ, T. -K. CHOU, C. ZHANG, K. NAJAFI, M. O. MULLER, L. P. BERNAL, P. WASHABAUGH 2000 A wafer-integrated array of micromachined electrostatically-driven ultrasonic resonators for microfluidic applications. Submitted to MEMS 2000 conference, January 23-27, 2000, Miyazaki, Japan..